JOURNAL OF SOLID STATE CHEMISTRY **129,** 22–29 (1997)
ARTICLE NO. SC967213

Crystal Growth of a Promising Nonlinear Optical Material: 2-Amino-5-Nitropyridinium Chloride

A. Ibanez,*,[1] J. P. Levy,* C. Mouget,* and E. Prieur[†]

* *CNRS Laboratoire de Cristallographie, associé à l'Université J. Fourier, B.P. 166, F-38042 Grenoble Cedex 09, France; and*
[†] *Exp. Div., European Synchrotron Radiation Facility, B.P. 220, F-38043 Grenoble Cedex, France*

Received April 11, 1996; accepted November 5, 1996

The experimental conditions of the synthesis and crystal growth of the 2-amino-5-nitropyridinium chloride (2A5NPCl) salt have been precisely determined, leading to the synthesis of large and optically clear crystals. Synchrotron X-ray diffraction topography shows that the crystalline quality of the samples is good and that most of the defects (grown-in dislocations) originate from the seed. This organic–inorganic phase, which exhibits a high nonlinear optical efficiency (powder tests), a large transparency range (410–2000 nm), suitable thermal, chemical, and mechanical stabilities, and a bulky habit, is a promising material for nonlinear optics.

1. INTRODUCTION

Due to their poor chemical stability and low thermal and mechanical resistances, nonlinear optical organic crystals are currently limited in their industrial applications. Recently, a crystal engineering strategy aimed at building very cohesive noncentrosymmetric frameworks based on host–guest chemistry has been proposed (1).

A highly polarizable organic molecule, 2-amino-5-nitropyridine (2A5NP), selected as guest, has been anchored onto various inorganic or organic anionic matrices. Short and multiple hydrogen-bonded networks observed in all these new organic–inorganic structures provide crystalline materials with improved thermal, chemical, and mechanical stabilities compared with those observed in molecular crystals built with the same chromophore. All the noncentrosymmetric structures of the 2-amino-5-nitropyridinium salts exhibit subnetworks of herringbone motifs of chromophores. The $(H_2PO_4^-)_n$ (2), $(H_2AsO_4^-)_n$ (3)], $(Cl^-)_n$ and $(Br^-)_n$ (4), $(C_4H_5O_6^-)_n$ (5, 6), $(CHCl_2COO^-)_n$ (7), and $(HPO_3CH_2COO^-)_n$ (8) host matrices, inducing noncentrosymmetric arrangements of chromophores, are chained or layered aggregates onto which the organic cations are strongly anchored.

The first qualitative characterization of second harmonic generation (SHG), carried out via powder tests (9) using a Nd:YAG laser at 1.06 μm, shows that the 2-amino-5-nitropyridinium chloride (2A5NPCl) and bromide (2A5NPBr) salts have high nonlinear optical efficiencies which are close to that of 2-methyl-2,4-dinitrophenyl aminopropanoate crystal (MAP) (10). This efficiency is probably due to the density of chromophores, which is the highest observed among the herringbone structures built with the 2-amino-5-nitropyridinium entity ($2A5NP^+$) (4). These materials, like the 2-amino-5-nitropyridinium dihydrogenphosphate (2A5NPDP) salt, are promising candidates for frequency doubling and optical parametric oscillation (OPO) (11, 12). Indeed, an OPO device having a low oscillating threshold (6 MW/cm^2) and a yield of 8% has been built recently with a 2A5NPDP crystal (13). For a complete crystal characterization (determination of macroscopic tensorial coefficients χ^2 and phase matching conditions) large crystals of high quality are needed. Thus, the growth of crystals of the 2A5NPCl salt has been undertaken.

Our first results obtained on this material, its synthesis, its solubility, and its crystal growth from solution are presented here. Then, a morphological study of the 2A5NPCl crystals is introduced. Finally, their transparency bandwidth and their microhardness are determined and their crystalline quality is investigated by synchrotron X-ray topography.

2. SYNTHESIS AND SOLUBILITY

The commercial (Jansen Chemicals, purity of 99%) 2-amino-5-nitropyridine ($C_5H_5O_2N_3$) powder is first purified by double sublimation. This organic compound is a weak Brønsted base which gains a proton in strong acidic aqueous solutions (pH < 2), leading to the dissolution of 2-amino-5-nitropyridine (2A5NP) in these solvents and the formation of salts with the conjugate bases of the involved acids. Thus, the 2A5NPCl salt is obtained by dissolving

[1] To whom correspondence should be addressed.

0022-4596/97 $25.00

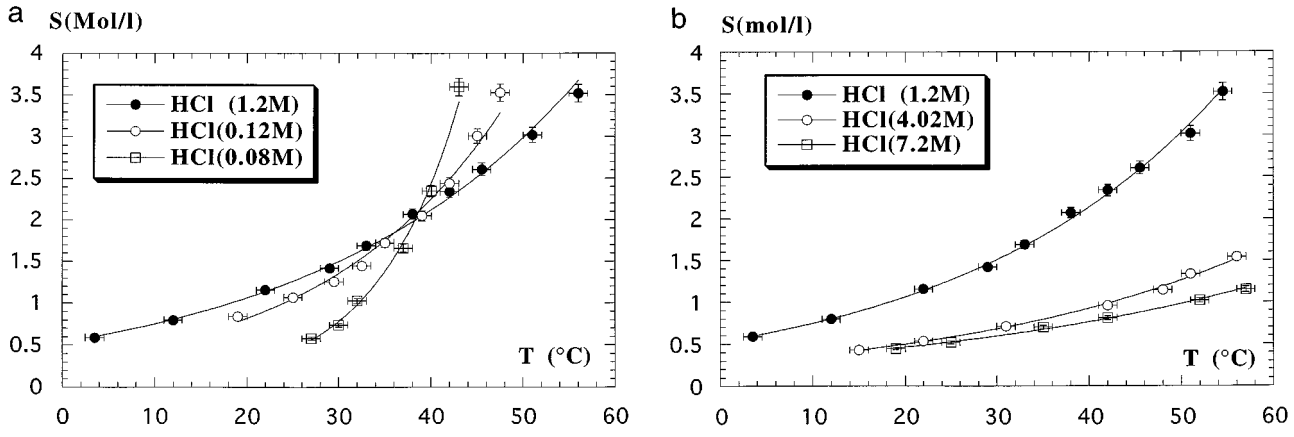

FIG. 1. Solubility curves of 2A5NPCl salt in hydrochloric acidic solvents: (a) HCl (0.08, 0.12, and 1.2 *N*) aqueous solutions, (b) HCl (1.2, 4, and 7.2 *N*) solutions.

2A5NP in a hydrochloric acid solution at 60°C with the molar ratio 1:2:8 for 2A5NP, HCl, and H_2O, respectively. This organic salt crystallizes at room temperature as a white microcrystalline powder by the addition of acetone. The synthesis yields are close to 100%. The material is purified again from HCl aqueous solution by a recrystallization in acetone. The purity of the first single crystals obtained from crystal growth has been monitored by energy dispersive X-ray analysis and X-ray fluorescence. These results do not indicate the presence of any significant impurity in the 2A5NPCl crystals.

Thermogravimetric analyses were carried out under air or N_2 at a heating rate of 1°C/min. These experiments have shown that the 2A5NPCl phase decomposes at temperatures over 150°C following the reactions

$$C_5H_6O_2N_3Cl \rightarrow C_5H_5O_2N_3 + HCl. \qquad [1]$$

Thus, the crystal growth of this material has been undertaken from solution. The necessity of stabilizing the $2A5NP^+$ cations in the solution (pH < 2) and the fact that the 2A5NP organic molecule gives salts with all the strong or medium acids ($pK_a < 3.3$) (1–8) led us to select hydrochloric acid as solvent. The magnitude of the 2A5NPCl solubility and its variation with temperature were determined for various HCl molar concentrations between 20 and 60°C (Figs. 1a and 1b). The 2A5NPCl salt exhibits always a high solubility and a positive solubility–temperature gradient (direct solubility) in these HCl solutions. The magnitude of the solubility is connected to the pH of the solution as shown in Fig. 2: the lower the pH value, the higher the solubility. Furthermore, the ratio of solubility–temperature gradient to solubility (solubility ratio) decreases when the HCl molarity increases (Fig. 3). From the measured solubility values, *S*, of the 2A5NPCl salt, log *S* was plotted versus $1/T$. The plots show that all the hydrochloric acid solutions obey the van't Hoff law within the

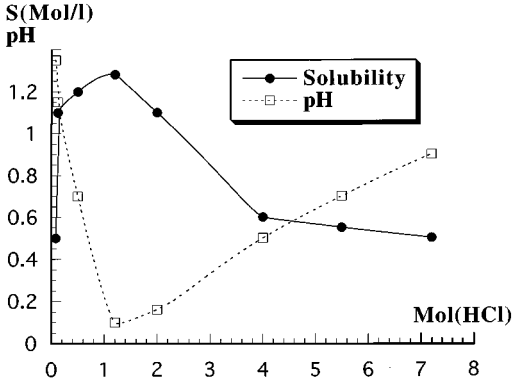

FIG. 2. Dependence of 2A5NPCl solubility at 26°C and of pH on HCl molarity.

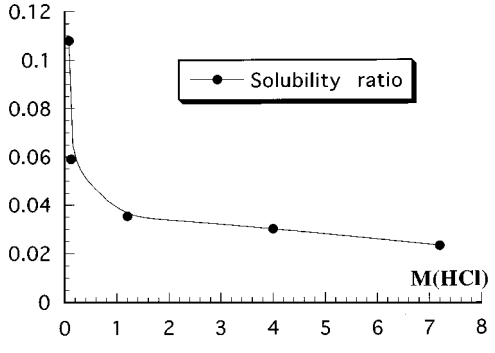

FIG. 3. The solubility ratio averaged between 35 and 45°C as a function of HCl molarity.

studied temperature range (0–60°C). For the concentrated hydrochloric acid solutions (1–7 *M*), a linearization of the data by a least-squares method gives a rather constant heat of dissolution of about 25 kJ/mol. These experimental results suggest that the dissolution reaction does not change and that it involves essentially the proton concentration. This can be described by the simplified equilibrium

$$C_5H_6O_2N_3Cl + H^+ \Leftrightarrow C_5H_6O_2N_3^+ + HCl. \quad [2]$$

The strong dependence of solubility–temperature curve of the 2A5NPCl salt on HCl molarity (Fig. 1) allows a flexible adjustment of crystal growth conditions.

3. CRYSTAL GROWTH

The choice of the growth method was based on the temperature-dependent solubility of 2A5NPCl in hydrochloric acid solutions. We have used the temperature lowering (TL) method for this material. For better control of the crystal growth, high HCl molar concentrations were selected here as solvent (HCl 4 to 7 *M*). Indeed, these acidic solutions have the lowest solubility–temperature gradients (Fig. 3). Nevertheless, the ratio of solubility–temperature gradient to solubility lies in the range 0.02–0.03 between 35 and 45°C (Fig. 3). Thus, when the TL method is used to obtain high-quality crystals, the temperature lowering rates must be always below 0.2°C per day at supersaturations around 0.01. This requires a high temperature precision ($\pm$ 0.002°C) to prevent rapid and uncontrolled bursts of growth leading to solvent inclusions or imperfections in the resulting crystals. We have developed a TL crystallization apparatus which contains several features contributing to the production of high-quality crystals. In order to have a high thermostatic control of the crystal growth close to $\pm$ 0.001°C, the vessel containing the growth solution is completely immersed in a 30-L bath of water regulated at $\pm$ 0.001°C. Furthermore, this external bath, the stirrers involving low-power electric motors (limitations of this parasitic heating), the immersion heater, and the temperature sensors (Pt: 100 Ω) are inserted in an isothermal box and located in a thermally controlled room ($\pm$ 5°C). A diagrammatic representation of this crystallizer is given in Fig. 4.

The growth solution is seeded using 2A5NPCl crystals about 1 mm^3 in size. These first seeds, carefully handled and selected with a polarizing microscope, were obtained by spontaneous nucleation resulting from the slow evaporation of saturated HCl (7 *M*) solutions. In order to obtain nondisturbed morphologies, the seeds are fixed by fusion to a thin platinum wire on low-growth-rate faces. They are then immersed into the solution and are lightly dissolved a few hours before the solution is equilibrated with an optical quality control. Both the seed holder and the stirring

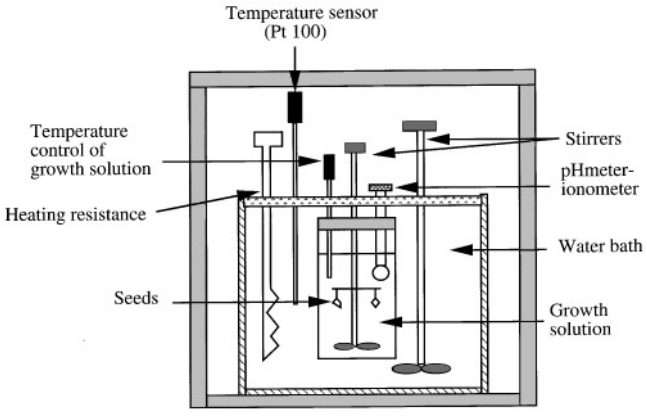

FIG. 4. Diagrammatic representation of the temperature lowering reactor.

paddle are rotated with speeds in the range 15–25 rpm and are reversed every 30 sec. The temperature is then decreased from about 45 to 35°C with a cooling rate of 0.004–0.006°C/h. Under these experimental conditions we have completely avoided the typical problems of solvent inclusion, veiling, and spurious nucleation that we have encountered during several trials carried out with temperature gradient methods. Thus, large (for example, $25 \times 12 \times 12$-mm^3 in Fig. 5a) and optically clear crystals are grown in 250–300 cm^3 of solution and from 3 to 6 seeds. These 2A5NPCl crystals are now suitable for the characterization of their nonlinear optical properties, which is in progress.

4. CRYSTAL MORPHOLOGY

The experimental growth morphology of 2A5NPCl crystals was determined from interfacial angle measurements using a two-circle optical goniometer (NEDINSCO). The 2A5NPCl crystals exhibit a rich morphology as shown in Fig. 6. This typical habit, obtained in hydrochloric acid solutions, does not change significantly with supersaturation or pH conditions. The 2A5NPCl phase grows in a number of well faceted forms, which are listed here in the order of their relative development: $\{1-10\}$, $\{110\}$, $\{001\}$, $\{221\}$, $\{22-1\}$, $\{331\}$, $\{33-1\}$, $\{100\}$, $\{201\}$, $\{20-1\}$, $\{210\}$, $\{111\}$, $\{11-1\}$, and $\{1-11\}$.

In agreement with the crystal structure, this nonsymmetric habit is induced by the relative growth rates listed in Table 1. The 2A5NPCl crystal morphology has been drawn with the program SHAPE (14), using the experimental growth rates as the face-crystal center in the Wulff plot. The dominating crystal form $(1-10)$ has the highest growth rate, which is about 0.7–0.8 mm/day under the experimental conditions presented above, while that of the opposing face (-110) corresponding to the $\{110\}$ form is insignificant. The high index forms $\{221\}$, $\{22-1\}$, $\{331\}$, and $\{33-1\}$, have

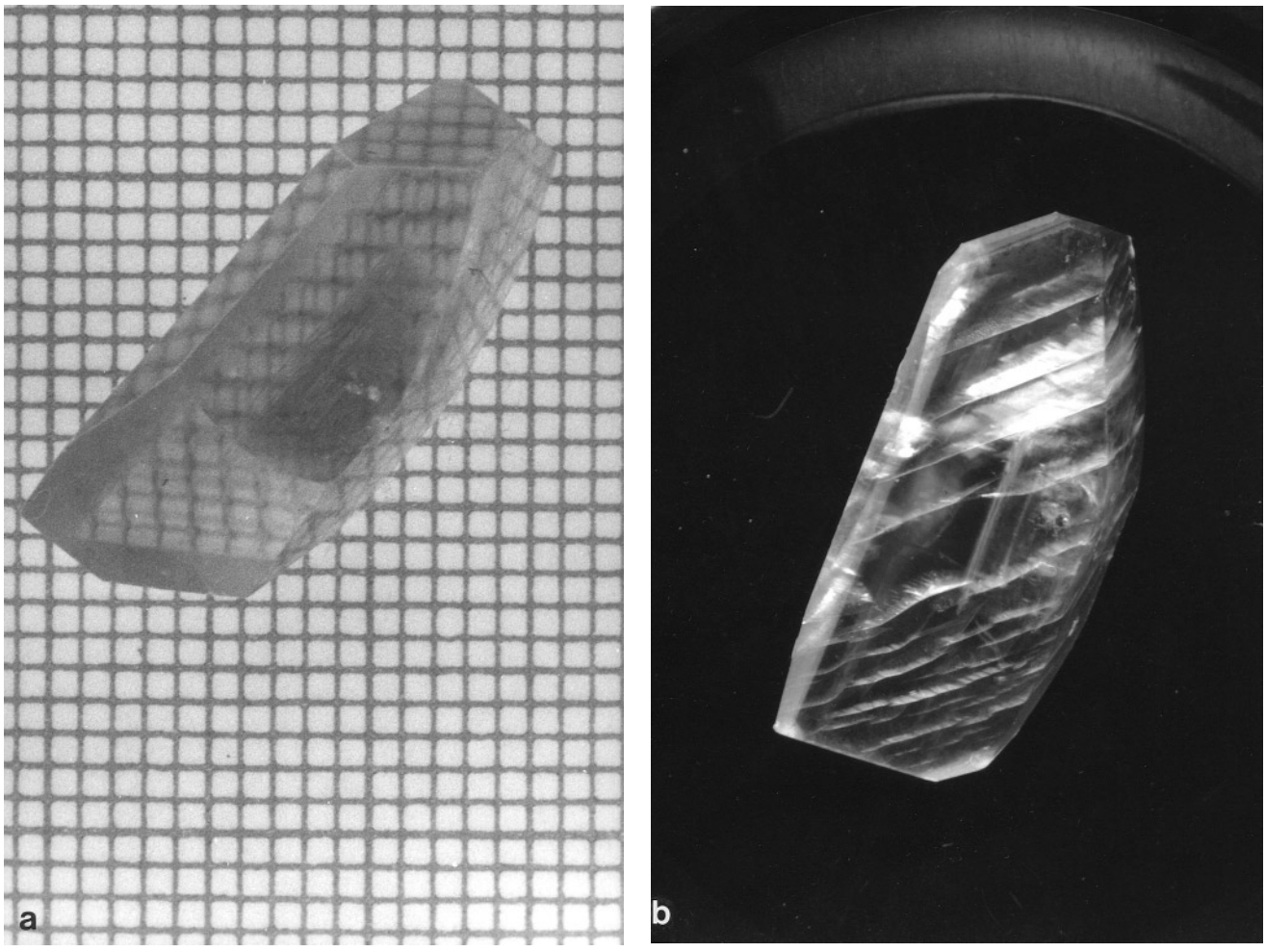

FIG. 5. (a) 2A5NPCl crystal ($0.9 \times 1.5 \times 2.0$ cm) grown in HCl (7.2 *N*) aqueous solution. (b) Preferential development of cracks in (201) planes on a quenched 2A5NPCl crystal ($1 \times 1.7 \times 2$ cm). The seeds are visible on the right sides of the crystals.

negligible growth rates, in contrast to the low index faces (100) and (001) (Table 1). The observed growth rates of the different faces can be summarized as follows: the right-hand dihedral forms [$\{110\}$, $\{111\}$, $\{11-1\}$, $\{221\}$, $\{22-1\}$, $\{331\}$, and $\{33-1\}$] do not grow significantly, while the left-hand dihedron $\{1-10\}$ and the pinacoids [$\{100\}$, $\{001\}$, $\{20-1\}$, and $\{201\}$] present large and similar growth rates, leading to a bulky crystal habit.

On the other hand, the 2A5NPCl crystals have a mechanical cleavage plane (100). Furthermore, they can be cracked along a preferential direction parallel to the (201) planes when they are quenched from 60 to 10°C by dipping in acetone (Fig. 5b). To prevent these thermal strains, the 2A5NPCl crystals are slowly cooled in the crystallizer, at the end of the growth experiment, just above the mother solution.

In order to explain all these experimental observations, the correlations existing between crystal structure and crystal morphology are being studied using the Hartmann–Perdock theory and computer morphological simulations based on the attachment energy concept (15–17).

5. CHARACTERIZATION OF GROWN CRYSTAL

5.1. Optical Transmission

The 2A5NPCl crystals are transparent and slightly green, as are the growth solutions, in agreement with the transparency range. The optical transmission spectrum of 2A5NPCl crystal shown in Fig. 7 was measured perpendicular to a 1-mm-thick (001) plate. A wide transmission band is observed in the near IR–visible region. The cutoff wavelength (defined at 50% transmittance) is 410 nm and is short enough for SHG of Nd : YAG laser radiation at 1.064 μm or other applications in the blue region as observed for 2A5NPDP (10–13). The change in the molecular charge

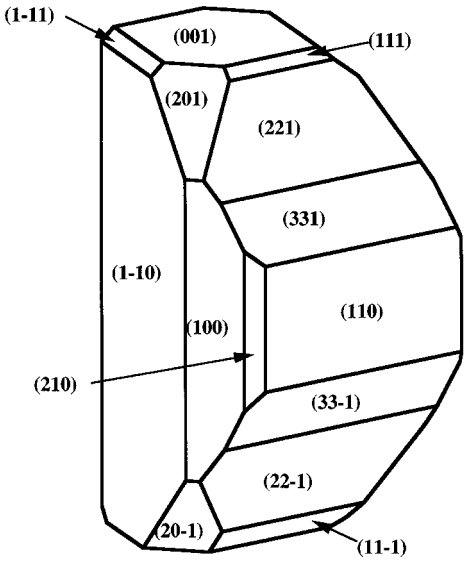

FIG. 6. Typical morphology of 2A5NPCl crystals as grown in HCl solutions.

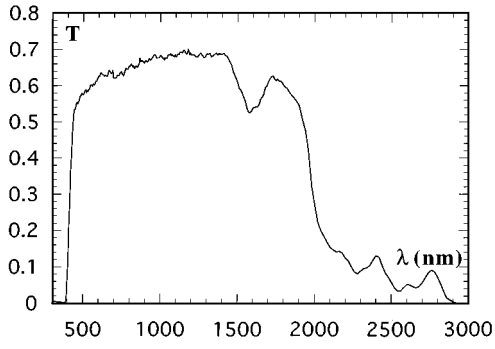

FIG. 7. Optical transmission spectrum of 2A5NPCl crystal measured normal to a (001) plate of 1-mm thickness.

transfer caused by the protonation of the 2A5NP molecule in the acid medium (pH < 2) induces an important shift of the λ cutoff (18) toward the near UV region (≈ 80 nm) compared with the 2A5NP molecule (yellow) and other pure organic molecular crystals (19). The protonation of the pyridine function certainly shifts the low-lying π–π^* transition of the aromatic ring toward higher energies (2). On the other hand, the weak absorption peak around 1650 nm can be ascribed to C–H bond overtone vibrations. The large absorption band starting near 2000 nm is typical of aromatic rings.

TABLE 1
Observed Crystal Forms and Their Corresponding Interplanar Spacing d_{hkl}, Experimental Growth Rates Relative to That of the $\{1-10\}$ Forms, Morphological Importance (M.I.)

$\{hkl\}$	d_{hkl}	r_{hkl}/r_{1-10}	M.I.
{100}	9.904	0.65	Moderate
{1−10}	6.0971	1	Large
{110}	6.0971	≈ 0	Large
{001}	4.7878	0.8	Large
{210}	4.1708	0.6	Small
{11−1}	3.8861	≈ 0	Small
{1−11}	3.6556	0.9	Small
{111}	3.6556	≈ 0	Small
{20−1}	3.6324	0.85	Moderate
{201}	3.2789	0.8	Moderate
{22−1}	2.6480	≈ 0	Large
{221}	2.5013	≈ 0	Large
{33−1}	1.9146	≈ 0	Moderate
{331}	1.8299	≈ 0	Moderate

5.2. *Microhardness Study*

Measurement of mechanical hardness was carried out using a Leitz Vickers hardness tester. Indentations were made on (110), (1 −10), and (001) plates with a dwelling time kept constant at 15 sec and weights ranging from 15 to 25 g. All these measurements gave an average value of 30 ± 5 kg/mm^2. The hardness of 2A5NPCl crystals is significantly lower than that of KDP (135 kg/mm^2), which implies that special care must be taken during processing and device fabrication. Nevertheless, these 2A5NPCl crystals can be suitably sliced and polished. The surface of 2A5NPCl single crystals is moisture sensitive following the decomposition reaction [1] but is stabilized under a dry atmosphere.

5.3. *Synchrotron X-Ray Diffraction Topography*

X-ray diffraction topography is an imaging technique widely used in characterizing crystalline defects in single crystals (20, 21). It has been applied mostly to semiconductors and metals but also to organic crystals (22). In most cases the X-ray source is a rotating anode. Compared to classical X-ray sources, the radiation from the so-called third-generation synchrotrons, such as ESRF (European Synchrotron Radiation Facility), has a photon intensity several orders of magnitude higher, very low divergence, and a continuous energy spectrum reaching hard X-ray or even gamma-ray energies (23). These characteristics make possible the study of thick and absorbing materials with very short exposure times (10^{-2}–10^2 sec) and with very high spatial resolution for diffracted images (≈ 1 μm). Furthermore, several diffraction topographs can be developed on one film in one exposure when polychromatic or white beam radiation is used (24). The topographs of the present study were recorded at the ESRF at D5 Optics beamline.

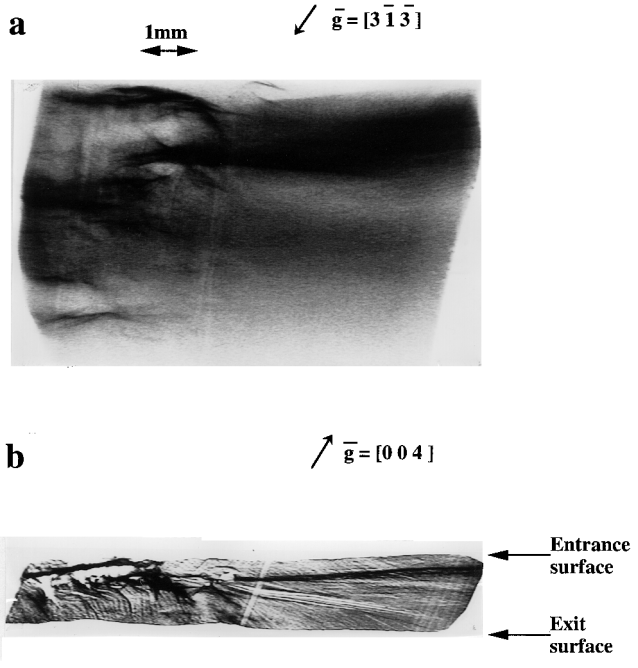

FIG. 8. (a) Transmission topograph and (b) section topograph of the 2A5NPCl crystal. The upper and the lower part of the (b) correspond to the entrance and the exit surfaces of the beam, respectively. The arrows indicate the direction of the diffraction vector $\bar{g}$. In (a) the wavelength of the diffracted beam $\lambda = 0.45$ Å, $\bar{g} = [3\,{-1}\,{-3}]$, and $\mu \cdot t = 1.0$, where μ is a linear absorption coefficient and t is the sample thickness. In (b) $\lambda = 0.40$ Å, $\bar{g} = [004]$, and $\mu \cdot t = 0.7$.

From the usable photon energy spectrum (about 6–80 keV) the lower part was filtered away, thus reducing the heat load on the sample which might influence image contrast or even damage the sample. All measurements were done in transmission (Laue) geometry either by using a wide beam (30×8 mm) or by limiting the beam vertically by a narrow (≈ 20 μm) slit. The latter technique is called section topography because only a small section of the sample diffracts. The resulting topograph gives information about the three-dimensional orientation of defects in this section. Because a smaller part of the sample is illuminated in section topography than in normal transmission topography, the defect images are more easily distinguished, especially in measurements of samples with rather high defect density such as the 2A5NPCl crystals examined here. For that reason the section technique was mainly used in this study.

Topographs were taken from five 2A5NPCl crystals of size on the order of several cubic centimeters. The synchrotron radiation did not damage the crystals in any sense. The topographs show that the crystals are of quite good crystalline quality and relatively similar. Figure 8a is a typical transmission topograph of the studied 2A5NPCl crystals and it shows that the biggest defects come from the seed. Defects are seen on the topographs as intensity variations. Contrast is mainly kinematic because $\mu \cdot t \leq 1$, where μ is a linear absorption coefficient and t is the sample thickness. Figure 8b is the section topograph of the same sample showing the defects propagating from the seed (upper left) to the right and down on the topograph. These defects are very likely so-called grown-in dislocations which nucleate at the crystal growth face. The usual origins of grown-in dislocations are inclusions at the surface of the seed crystal or accidents during growth. In Fig. 8a the high density of the defects, due to the sample thickness (≈ 12 mm), prevents their detailed investigation, in contrast to the section topograph (Fig. 8b). In this latter case, the lines parallel to the diffraction vector are an artifact related to phase contrast of small dust particles in the slit (25).

Figure 9 shows a series of section topographs from a 2A5NPCl crystal. Figures 9a–9d are all taken under the same conditions, but between the exposures the crystal was moved up by 3 mm along the (001) axis (Fig. 9f). In Fig. 9d the seed is clearly visible in the upper left of the topograph. The white area around the seed corresponds to a very deformed region which does not diffract or to a misoriented region which diffracts radiation in a direction differing from other parts of the sample (topographs were taken using white radiation). As the distance from the seed increases, the crystalline quality of the sample improves significantly, and 9 mm above the seed (Fig. 9a) the topograph shows no more large defects. This part of the sample is of the highest crystalline quality and could be used as a seed crystal in a following growth. Figure 9e is taken from the same crystal but in this case it was tilted 90°. The propagation of the defects (very likely grown-in dislocations) from the seed is clearly visible.

6. CONCLUSIONS

The 2A5NPCl salt showing a high nonlinear optical efficiency, associated with a transparency bandwidth from 410 to 2000 nm, with suitable thermal, chemical, and mechanical stabilities and with a bulky crystal habit, is a promising candidate for frequency doubling and optical parametric oscillation. The experimental conditions of the synthesis and crystal growth have been well determined, leading to the production of large (several cm^3) and optically clear crystals.

Synchrotron X-ray diffraction topography proved to be a valuable characterization method for the 2A5NPCl crystals. The measurements showed that the general crystalline quality of the samples is good and significantly better than that typically observed in organic crystals (22). Most of the defects originate from the seed and propagate through the sample. It is assumed that they are grown-in dislocations. In order to increase the crystal quality, we will use as seed (001) crystals cuts of the highest crystalline quality (Fig. 9a)

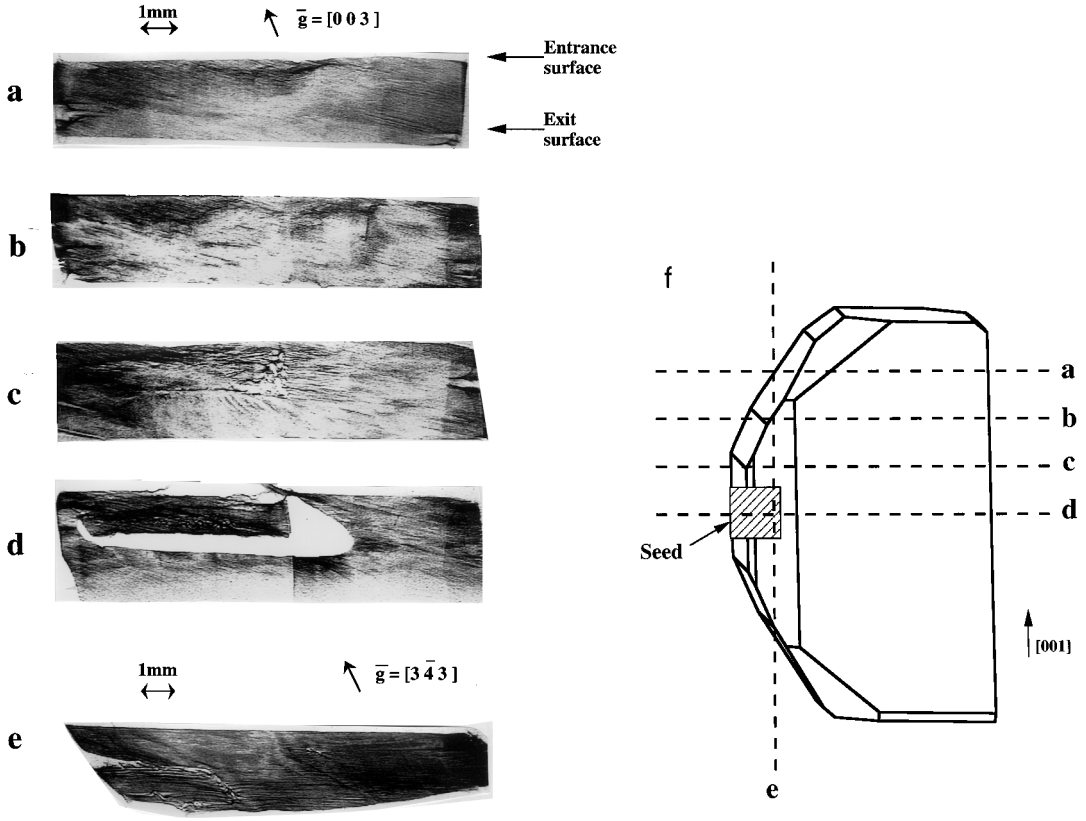

FIG. 9. Section topographs of the 2A5NPCl crystal. Topographs are taken (a) 9 mm, (b) 6 mm, (c) 3 mm above the seed area and (d) from the seed area, $\lambda = 0.33$ Å, $\bar{g} = [003]$, and $\mu \cdot t = 0.4$. (e) Section topograph of the sample but tilted 90°. The seed is visible in the left side. $\lambda = 0.37$ Å, $\bar{g} = [3\text{–}43]$, and $\mu \cdot t = 0.6$. The locations of the different section topographs are represented by dotted lines in (f).

among the studied samples, instead of the initial millimeter-sized crystals grown by slow evaporation used in this work. These (001) plates will be sawed in a strain-free way using an acid saw. Furthermore, morphological modeling of 2A5NPCl using the attachment energy concept is under way.

ACKNOWLEDGMENTS

The authors thank Drs. René Masse (Laboratoire de Cristallographie, CNRS Grenoble) and José Baruchel (ESRF Grenoble) for fruitful discussions, Dr. Andreas Freund for beam time at the D5 Optics beamline as ESRF, and Dr. E. Bustarret (LEPES, CNRS Grenoble) for the IR characterization.

REFERENCES

1. R. Masse, M. Bagieu-Beucher, J. Pécaut, J. P. Lévy, and J. Zyss, *Nonlinear Opt.* **5,** 413 (1993).
2. R. Masse and J. Zyss, *Molec. Eng.* **1,** 141 (1991).
3. J. Pécaut, Y. Le Fur, and R. Masse, *Acta Crystallogr. Sect. B* **49,** 535 (1993).
4. J. Pécaut, J. P. Lévy, and R. Masse, *J. Mater. Chem.* **3,** 999 (1993).
5. J. Zyss, R. Masse, M. Bagieu-Beucher, J. P. Lévy, *Adv. Mater.* **5,** 120 (1993).
6. O. Watanabe, T. Noritake, Y. Hirose, A. Okada, and T. Kurauchi, *J. Mater. Chem.* **3,** 1053 (1993).
7. Y. Le Fur, M. Bagieu-Beucher, R. Masse, J. F. Nicoud, and J. P. Lévy, submitted for publication.
8. J. Pécaut and R. Masse, *J. Mater. Chem.* **4,** 1851 (1994).
9. S. K. Kurtz and T. T. Perry, *J. Appl. Phys.* **39,** 3798 (1968).
10. J. L. Oudar and R. Hierle, *J. Appl. Phys.* **48,** 2699 (1977).
11. Z. Kotler, R. Hierle, D. Josse, J. Zyss, and R. Masse, *J. Opt. Soc. Am. B* **9,** 534 (1992).
12. I. D. W. Samuel, B. Villacampa, D. Josse, S. Khodja, and J. Zyss, *Appl. Phys. Lett.* **66,** 2019 (1995).
13. S. Kodja, "Interaction paramétrique optiques dans les cristaux organiques et organo-minérauz," Thèse de l'école Polytechnique en Sciences Physique, Palaiseau, France, 1995.
14. E. Dowty, SHAPE, 521 Hidden Valley Road, Kingsport, TN 37663, 1989.
15. P. Hartmann and W. G. Perdock, *Acta Crystallogr.* **8,** 49 (1995).
16. P. Hartmann, *in* "Crystal Growth: An Introduction" (P. Hartmann, Ed.), p. 367, North-Holland, Amsterdam, 1973.
17. G. Clydesdale, R. Docherty, and K. J. Roberts *Comp. Phys. Comm.* **64,** 311 (1991).
18. M. Dewar, *J. Chem. Soc.* 2329 (1950).
19. J. Zyss, J. F. Nicoud, and M. Coquillary, *J. Chem. Phys.* **81,** 4160 (1984).
20. B. K. Tanner, "X-ray Diffraction Topography," Pergamon Elms Pord NY (1976).

21. J. Baruchel, *in* "Neutron and Synchrotron Radiation for Condensed Matter Studies: Theory, Instruments and Methods, HERCULES" (J. Baruchel, J. L. Hodeau, M. S. Lehmann, J. R. Regnard, and C. Schlenker, Vol. 1, p. 399, Editions de Physique/Springer-Verlag, Berlin, New York, 1993.
22. H. Klapper, *in* "Crystals," Vol. 13, p. 109, Springer-Verlag, Berlin (1991).
23. T. Tuomi, K. Naukkarinen, and P. Rabe, *Phys. Stat. Sol.* (*a*) **25,** 93 (1974).
24. J. Miltat, *in* "Characterization of Crystal Growth Defects by X-ray Methods" (B. K. Tanner and D. K. Bowen, Eds.), p. 401, Plenum, New York, 1980.
25. P. Cloetens, R. Barrett, J. Baruchel, J. P. Guigay, and M. Schlenker, *J. Phys. D Appl. Phys.*, in press.